Application of Duffing Oscillators for Passive Islanding Detection of Inverter-Based Distributed Generation Units

Hesan Vahedi, *Student Member, IEEE*, G. B. Gharehpetian, *Senior Member, IEEE*, and Mehdi Karrari

***Abstract*—Regarding the safety and reliable operation of modern distributed generation (DG) systems, an expert diagnosis apparatus is required to distinguish between different events. One of the crucial requirements in DG safe operation is the "islanding detection." In this paper, a new passive islanding detection method, based on the application of the Duffing oscillators, is suggested for the first time and tested under different network conditions. The method is designed to detect the changes on point of common coupling frequency by identifying the transformation of the Duffing oscillator from "chaotic state" to "great periodic state" and vice-versa. The simulations results, carried out by MATLAB/Simulink, are used to validate the performance of the proposed method. It is shown that the proposed method has excellent accuracy within a minimum detection time, even with the presence of high noise to signal ratios.**

***Index Terms*—Chaos, distributed generation (DG), duffing equation, islanding, voltage source converter.**

I. Introduction

ISLANDING operation of distributed-generation (DG) units usually occurs when the power supply is disconnected from the main utility but the DG keeps supplying power into the network. Failure to trip the DG during islanding may produce several negative impacts on DG equipment and utility power systems. The DG unit should detect the islanding and disconnect the DG unit in a timely manner to avoid damages [1], [2]. The main part of islanding detection is to accurately discern the moment of islanding and isolate the DG from the distribution network (DN) in minimum time. Unintentional islanding of DG may result in power-quality (PQ) issues, interference with grid protection devices, and low safety for consumers. It should be mentioned that some researchers are investigating the situation in which the DG has the ridethrough capability and is authorized to energize the load after islanding [3]–[6]. This option can add more complexity to the control system and costs as well.

In general, islanding detection methods are categorized into three main groups; namely: passive, active, and communication-based methods [7]. Passive islanding detection methods estimate the moment of the islanding using different measurements at the PCC. This benefit of passive methods is wane due to the fact that it is not easy to rely only on system parameters (e.g., voltage and frequency) for accurate detection of the islanding instant. Differentiating the system contingencies and transients from those of islanding events is not easy. Setting upper and lower thresholds can help to discriminate between the islanding and grid-connected conditions. However, this results in large nondetection zones (NDZs). For example, the over/underfrequency protection method uses upper and lower frequency thresholds. Sometimes, the load closely matches the DG capacity. In this case, the amount of the frequency or voltage deviation will not be sufficient to trigger the islanding detection system. NDZ is defined by the load consumption and power generation conditions that cause failure to detect islanding in a timely manner. Passive islanding detection methods mostly suffer from large NDZs [8], [9]. Several passive islanding detection methods are available like: undervoltage/overvoltage protection (UVP/OVP) and underfrequency/overfrequency protection (UFP/OFP) [9]; rate of change of active power [10], [11]; rate of change of frequency (ROCOF) [12], [13]; rate of change of frequency over power [14]; voltage and power factor changes [15]; phase jump detection [16]; as well as voltage unbalance and total harmonic distortion [17].

Unlike passive islanding detection methods, active islanding detection schemes make a perturbation into the voltage-source converter (VSC) output current by injecting an active signal in order to cut off the power balance between DG and local load consumption [18]. Hence, it becomes easy to detect the islanding condition. The main advantage of these methods over passive detection methods is their relatively small NDZ [9]. However, most active schemes have disadvantages of complex structure, and PQ degradation, to some extent. Some renowned active methods include slide-mode frequency shift (SMS) [19], active frequency drift (AFD) [20], and Sandia frequency shift (SFS) [21]. Communication-based methods rely on sending and receiving signals between different measurement units and protection apparatus to detect islanding. A comprehensive survey on different islanding detection methods can be found in [7].

This paper proposes a new passive islanding detection method, which has a tiny NDZ and excellent accuracy. The proposed method is based on a virtue of signal processing using Duffing oscillators. The Duffing equation is applied because it is one of the classic nonlinear systems that has been extensively studied [22]–[24]. The basic idea is that a small periodic signal in a noise can be detected by the Duffing oscillator via a transition from the "chaotic motion" to "great periodic motion"

Manuscript received September 08, 2011; revised March 22, 2012 and June 18, 2012; accepted July 29, 2012. Date of current version September 19, 2012. Paper no. TPWRD-00764-2011.

The authors are with the Electrical Engineering Department, Amirkabir University of Technology, Tehran 15914, Iran (e-mail: h.vahedi@aut.ac.ir; grptian@aut.ac.ir; karrari@aut.ac.ir).

Digital Object Identifier 10.1109/TPWRD.2012.2212251

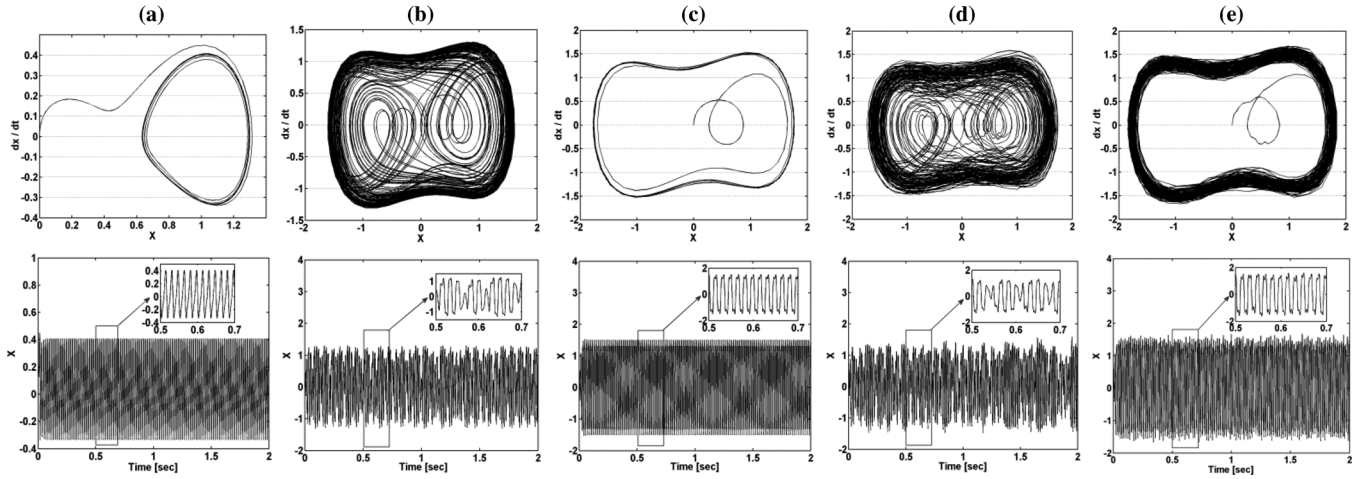

Fig. 1. Duffing oscillator in the phase plane and $x-t$ diagram. (a) Small periodic motion. (b) Chaotic motion. (c) Great periodic motion. (d) Chaotic motion additional Gaussian noise. (e) Great periodic motion-added Gaussian noise.

and vice-versa. The accuracy of the method is tested under a variety of conditions, including load switching, different load quality factors, and imbalance loading conditions. The sensitivity analysis of the presented method to the noise and comprehensive investigation on the NDZ of the method is also studied in this paper.

This paper is organized into the following sections: the next section illustrates the fundamental principle of Duffing oscillators. Section III presents the system under study. The proposed islanding detection method is discussed in Section IV. The performance of the presented method is evaluated in Section V and the paper ends with conclusions in Section VI.

II. Duffing Oscillators

Chaos describes the complex behavior of a nonlinear deterministic system. The first description of a chaotic process was made in 1963 by Lorenz [23]. Generally, a nonlinear dynamic system has four states: 1) the fixed point; 2) the periodic motion; 3) the chaotic motion; and 4) the quasiperiodic motion (great periodic motion). The basic idea of the signal detection scheme based on chaotic oscillators is that a small periodic signal in noise can be detected by the Duffing oscillator via a transition from chaotic motion to periodic motion.

The normal form of the Duffing equation is as follows:

$$\frac{d^2x}{dt^2}+\delta\frac{dx}{dt}-x+x^3=\gamma\cos(t) \tag{1}$$

where δ is the damping ratio, the term "$-x+x^3$" represents the nonlinear restoring force, and $\gamma\cos(t)$ is the periodic driving force. Assuming $y=dx/dt=\dot{x}$, we have [22]

$$\begin{aligned}\dot{x}&=y\\ \dot{y}&=-\delta y+x-x^3+\gamma\cos(t).\end{aligned} \tag{2}$$

If δ is fixed, then as γ varies from small to large, the system state varies from small periodic motion [Fig. 1(a)] to chaotic motion [Fig. 1(b)] and, at last, to the great periodic motion [Fig. 1(c)] [22] and [24].

If $\gamma=\gamma_c$ (γ_c refers to the critical value), then the system is in the critical state (chaos, but about to change to the periodic motion). The to-be-detected signal (D_f) can be viewed as a perturbation of the main sinusoidal driving force $\gamma\cos(t)$ (the reference signal). Although noise may be intense, it can only affect the local trajectory on the phase plane diagram, without causing any phase transition [Fig. 1(d) and (e)] [22]. In order to use (2) to detect weak signals with different frequencies, some frequency transformation should be applied. Considering $t=\omega\tau$, we have [22]

$$\begin{aligned}x(t)&=x(\omega\tau)=x^*(\tau)\\ \frac{dx(t)}{dt}&=\frac{1}{\omega}\frac{dx(\omega\tau)}{d\tau}=\frac{1}{\omega}\frac{dx^*(\tau)}{d\tau}\\ \frac{d^2x(t)}{dt^2}&=\frac{1}{\omega^2}\frac{d^2x(\omega\tau)}{d\tau^2}=\frac{1}{\omega^2}\frac{d^2x^*(\tau)}{d\tau^2}.\end{aligned} \tag{3}$$

Substituting (3) into (2), omitting the subscript $*$ of $x^*(\tau)$, and adding the input signal [22], we obtain

$$\begin{aligned}\dot{x}&=\omega y\\ \dot{y}&=\omega(-\delta y+x-x^3+\gamma_c\cos(\omega\tau)+\text{Input})\end{aligned} \tag{4}$$

where

$$\text{Input}=S(\tau)+\sigma(\tau)=a\cos\left((\omega+\Delta\omega)\tau+\varphi\right)+\sigma(\tau). \tag{5}$$

where $\sigma(\tau)$ is the Gaussian noise, $\Delta\omega$ is the frequency difference, and φ is the primary phase difference. In this paper, the fourth-order Runge–Kutta algorithm is used to solve the Duffing equation. Therefore, the system is a discrete dynamic system by nature. The dynamics of the discrete system are similar, but slightly different from the original continuous system. There is truncation error (discretization error) involved in a Runge–Kutta algorithm. It exists even with high precision arithmetic, because it is caused by truncation of the infinite Taylor series to form the algorithm [22]. Truncation error depends on the step size used, and the dependence is especially distinct, when the system is strongly nonlinear.

In this paper, $\delta=0.5$ and $h=10^{-5}$ (step size) were assumed and the value of γ_c was fixed at 0.81.

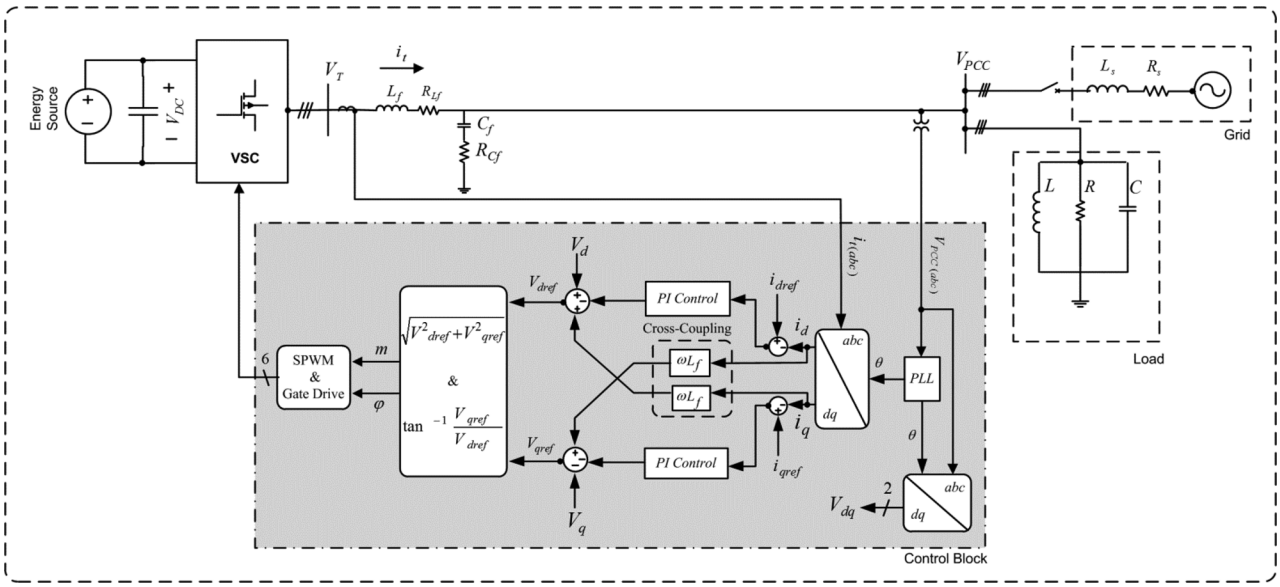

Fig. 2. System under study.

III. System Overview

The inverter-based DG under study is shown in Fig. 2. This system consists of a distribution network, modeled by a three-phase voltage source; a load, modeled by a three-phase constant impedance; and a photovoltaic (PV) system. The rating of this system is 100 kW and the other parameters are given in the Appendix. Fig. 2 also shows the control scheme based on the "dq" synchronous reference frame. In this system, the control strategy specifies the d- and q-axis components of the inverter output current corresponding to the real and reactive output power components, respectively. The figure also reveals that the d-axis and q-axis current components of the inverter are extracted through an "abc" to "$dq0$" transformation. The results are then compared with the corresponding reference signals that can be specified by external power or voltage-control loops. In this paper, the reference signals are set out directly to resemble the constant current control strategy. Then, the error signals are applied to two proportional-integral (PI) controllers. The outputs of these controllers deliver the reference voltages for the PWM signal generator. Another important feature of the current control strategy is the limitation of the inverter output current during a fault condition, providing overcurrent protection and reducing the fault current contribution of the unit. More details about the system can be found in [25].

IV. Proposed Method

In this section, a Duffing oscillator is designed to estimate the moment of the islanding in the system. The Duffing oscillator must have an input signal, which is combined with the (D_f) signal. In order to detect the islanding condition, the γ_c is set to a constant value to make the oscillator work at the chaotic state. Then, after the occurrence of an islanding event, the (D_f) signal (which is injected from the system to the Duffing input signal), can change the state of the oscillator from the chaotic motion to the great periodic motion and vice-versa.

A. Input Signal to the Duffing Oscillator

In the proposed method, to form the input signal, first the frequency deviation must be defined as follows:

$$D_f = \Delta f_0 + k_f \underbrace{|f - f_0|}_{|\Delta f|} \tag{6}$$

where Δf_0 is the offset value of the frequency deviation, "k_f" is the gain factor of the frequency deviation, "f" is the system frequency, and "f_0" is the system nominal frequency. Then, the input signal can be expressed by the following equation:

$$\text{Input} = D_f \cos(\omega\tau). \tag{7}$$

Fig. 3 shows the flowchart of the proposed islanding detection method including the Duffing oscillator model. As shown in the Duffing oscillator model, the input signal is added to the driving force (introduced in Section II) to be fed to the Duffing oscillator for monitoring the system condition. Considering (6), in the grid-connected mode, the value of Δf is negligible due to grid control over system frequency and cannot make a transition in the Duffing oscillator. In contrast, while the system is in the islanded mode, f would drift from the nominal value caused by grid absence. The gain factor k_f is multiplied by Δf to provide sufficient signal strength for a transition in the Duffing oscillator.

B. Duffing Oscillator Analysis

In this section, the Melnikov method is used to calculate the threshold value of the Duffing oscillator. When δ and γ are set to zero in (2), the equation represents a double well Duffing-type oscillator with $(x, y) = (0, 0)$, a degenerate saddle point and a single well Duffing-type oscillator with $(x, y) = (\pm 1, 0)$ two

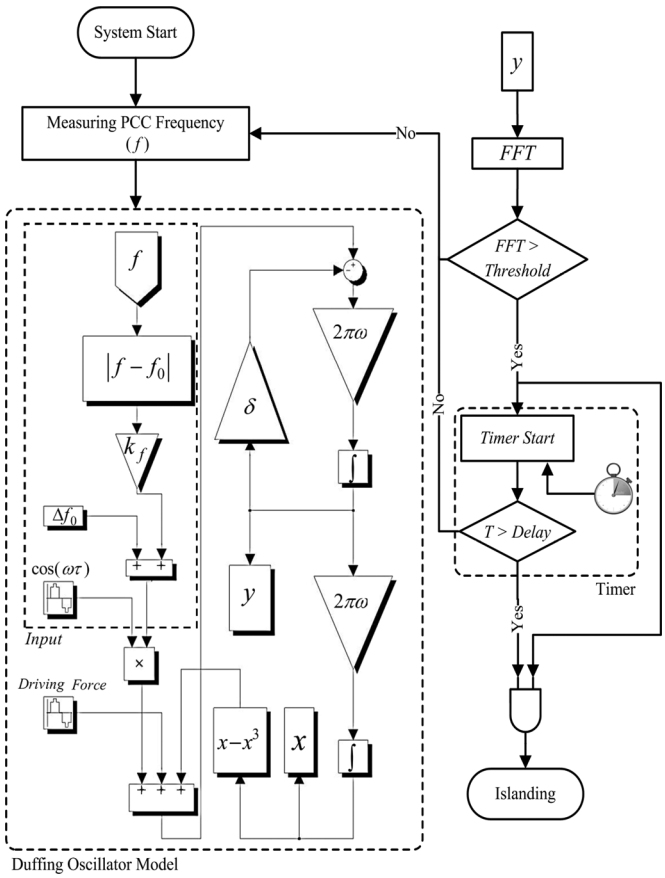

Fig. 3. Flowchart of the proposed Duffing oscillator.

degenerate saddle points [24]. In this case, (2) can be written as [24]

$$\begin{cases} \dot{x} = y \\ \dot{y} = x - x^3 \end{cases}. \tag{8}$$

Equation (8) is a completely integrable Hamiltonian system, and the level set of this equation can be written as follows [24]:

$$H(x,y) = \frac{y^2}{2} - \frac{x^2}{2} + \frac{x^4}{4} = 0 \tag{9}$$

which includes two homoclinic orbits Γ_0^+, Γ_0^- and a point $p_0 = (0,0)$. The unperturbed homoclinic orbits are given by the following equations [24]:

$$\begin{aligned} q_0^+ &= \left(+\sqrt{2}\,\mathrm{sec}\,h(t), -\sqrt{2}\,\mathrm{sec}\,h(t).\tanh(t)\right) \\ q_0^- &= \left(-\sqrt{2}\,\mathrm{sec}\,h(t), +\sqrt{2}\,\mathrm{sec}\,h(t).\tanh(t)\right). \end{aligned} \tag{10}$$

From the perspective of $q_0^{\pm}(0) = (\pm\sqrt{2}, 0)$, unperturbative homoclinic orbits are given as follows:

$$\begin{aligned} x_0 &= \left(\pm\sqrt{2}\,\mathrm{sec}\,h(t)\right) \\ y_0 &= \left(\pm\sqrt{2}\,\mathrm{sec}\,h(t).\tanh(t)\right). \end{aligned} \tag{11}$$

To compute the parameter values, for which a transverse crossing occurs, we have the Melnikov function

$$\begin{aligned} M(t_0) &= \int_{-\infty}^{\infty} y_0(t)\left(\gamma\cos\omega(t+t_0) - \delta y_0(t)\right)dt \\ &= -\sqrt{2}\cdot\gamma\int_{-\infty}^{\infty}\left(\mathrm{sec}\,h(t)\cdot\tanh(t)\cdot\cos\omega(t+t_0)\right)dt \\ &\quad - 2\delta\int_{-\infty}^{\infty}\left(\mathrm{sec}\,h^2(t)\cdot\tanh^2(t)\right)dt. \end{aligned} \tag{12}$$

Using the direct integration and the residue theory, we have

$$M(t_0,\gamma,\delta,\omega) = -\frac{4}{3}\delta + \sqrt{2}\cdot\gamma\cdot\frac{\pi\omega\sin(\omega t_0)}{\cosh\left(\frac{\pi\omega}{2}\right)}. \tag{13}$$

Letting

$$\alpha_1 = -\frac{4}{3}, \quad \alpha_2 = \sqrt{2}\pi\omega\,\mathrm{sec}\,h\left(\frac{\pi\omega}{2}\right). \tag{14}$$

If chaotic state occurs, $M(t_0,\gamma,\delta,\omega) = 0$ must have the solution, so the following equation can be obtained:

$$\alpha_1\delta + \alpha_2\gamma\sin(\omega t_0) = 0. \tag{15}$$

Therefore

$$\left|\frac{\alpha_1\delta}{\alpha_2\gamma}\right| = |\sin(\omega t_0)| \le 1. \tag{16}$$

And because of $dy(t_0)/dt_0 \neq 0$, $|\sin(\omega t_0)| \neq 1$ can be obtained. So, we have

$$\frac{\gamma}{\delta} = \frac{\alpha_1}{\alpha_2}. \tag{17}$$

The following bifurcation threshold for $q_0^+(t)$ or $q_0^-(t)$ can be obtained, as follows [24]:

$$\frac{\gamma}{\delta} = \frac{4\cosh\left(\frac{\pi\omega}{2}\right)}{3\sqrt{2}\pi\omega}. \tag{18}$$

The threshold values that can enter the system into a chaos state as well as a great periodic state can be calculated, while δ is established. When the value of δ is fixed, the system will change regularly with the change of γ. Now, let $\omega = 1$ and $\delta = 0.5$, the parameter γ is gradually increased from zero. Using (18), for $\gamma > 0.3765$, the system will appear in the chaotic state.

For the typical system of (2), the threshold value for entering into the great periodic motion is numerically determined ($\gamma_{th} = 0.8275$). The γ can be set to a value a little smaller than the critical value (γ_{th}). So the system is put into the critical state (chaos, but on the verge of changing to the great periodic motion). The system state changes from the periodic state to chaos state are very slow; while the system changes into the great periodic from the chaos state are very fast. So the latter domain is selected for the detection of islanding phenomenon.

C. Analysis of the Proposed Method

Using (4) and (5), it can be said that the total driving force of the Duffing oscillator is as follows [22], [23]:

$$\begin{aligned} A(t) &= \gamma_c \cos(\omega_0 \tau) + a\cos\left((\omega_0 + \Delta\omega)\tau + \varphi\right) \\ &= \gamma_c \cos(\omega_0 \tau) + a\cos(\omega_0 \tau)\cos(\Delta\omega + \varphi) \\ &\quad - a\sin(\omega_0 \tau)\sin(\Delta\omega + \varphi) \\ &= (\gamma_c + a\cos(\Delta\omega + \varphi))\cos(\omega_0 \tau) \\ &\quad - a\sin(\omega_0 \tau)\sin(\Delta\omega + \varphi) \\ &= \gamma(t)\cos\left(\omega_0 \tau + \theta(\tau)\right) \end{aligned} \tag{19}$$

where

$$\gamma(t) = \sqrt{\gamma_c^2 + 2\gamma_c a\cos(\Delta\omega + \varphi) + a^2} \tag{20}$$

$$\theta(\tau) = arctg\frac{a\sin\Delta\omega + \varphi)}{\gamma_c + a\cos(\delta\omega\tau + \varphi)}. \tag{21}$$

From (20), we can draw the following conclusion that if $\Delta\omega$ is equal to zero, then $\gamma = \sqrt{\gamma_c^2 + 2\gamma_c a\cos(\varphi) + a^2}$. Since γ_c is kept constant, the parameter a (the amplitude of the D_f signal) plays an important role to change the state of the Duffing oscillator. From (6), we have

$$a = \Delta f_0 + k_f|\Delta f|. \tag{22}$$

By combining (20) and (22) for $\Delta\omega = 0$ and $\varphi = 0$, we have

$$\gamma = \sqrt{\gamma_c^2 + 2\left(\gamma_c \Delta f_0 + k_f(\gamma_c \Delta f + \Delta f \Delta f_0)\right) + \Delta f_0^2 + k_f^2 \Delta f^2}. \tag{23}$$

In (23), the terms $\Delta f \Delta f_0$ and Δf_0^2 are relatively small and can be neglected. Fig. 4(a) shows the effect of the change in Δf_0 on the (D_f) signal. In this figure, the highlighted arrow shows the impact of the increase in Δf_0 on the Duffing oscillator input signal amplitude (D_f). This figure also reveals that by increasing Δf_0, the Duffing oscillator could be very sensitive to the changes in the (D_f) signal. Moreover, sensitivity analysis with changing k_f in (23) is shown in Fig. 4(b).

The deployed parameters for the proposed Duffing oscillator are listed in Table I. Some of the parameters $(\gamma_c, \gamma_{th}, \delta)$ were calculated based on mathematical evaluations, as described in the previous sections. The best values for other parameters were found by trial and error (using the results in Fig. 4).

D. Trip Signal Extraction

In the proposed method presented in this paper, the extraction of the trip signal is based on the fast Fourier transform (FFT) analysis of the Duffing oscillator output (y). The extracted command signal can be further used for deactivation or changing operation mode of the DG.

The Duffing oscillator output (y) signal waveform is symmetrical during the great periodic motion; but unsymmetrical during chaotic motion. For symmetrical waveforms, the even coefficients of FFT are almost zero. In contrast, for unsymmetrical waveforms, both even and odd coefficients are greater than zero. This fact was the key point to detect different modes in the Duffing oscillator. Moreover, many simulation results (some presented in Section V of the paper) revealed that the 3rd harmonic of the y signal has the greatest percentage of the magnitude in the great periodic and chaotic state of the Duffing oscillator.

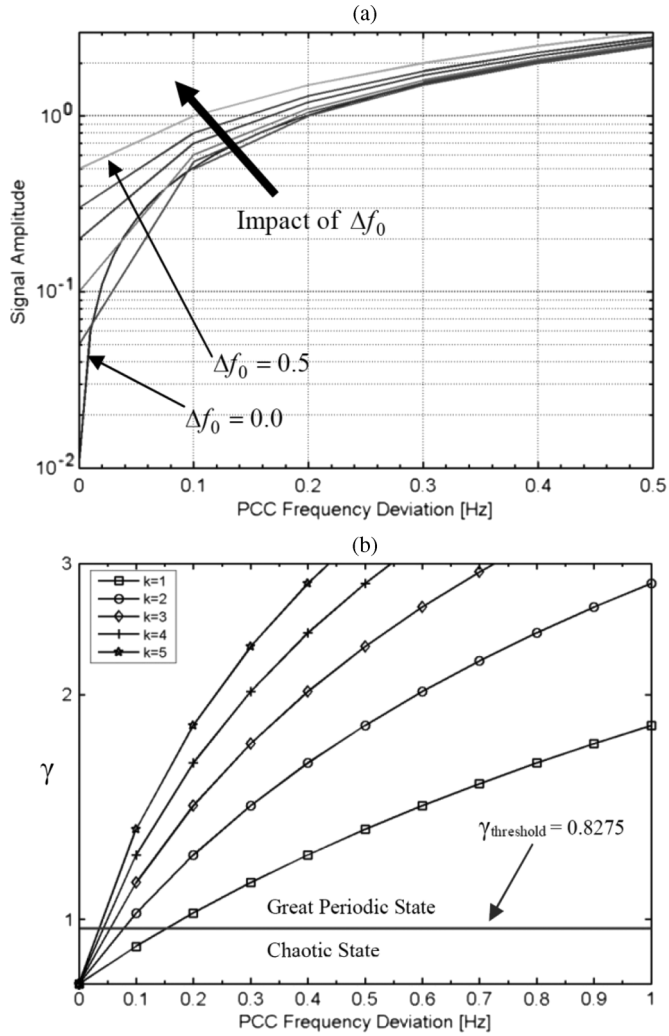

Fig. 4. PCC frequency deviation ($\gamma_{c=0.81}$, $k_f = [0.5 : 0.2 : 5]$, $k_f = [1 : 1 : 5]$, and $\Delta f = [0 : 0.01 : 1]$). (a) Amplitude of the injected signal. (b) γ.

TABLE I
PROPOSED METHOD PARAMETERS

Parameter	k_f	Δf_0	γ_c	γ_{th}	δ
Value	5	0.01	0.81	0.8275	0.5

Based on these points, the difference between the 3rd harmonic from the 4th harmonic of the y signal proved to be the best criteria to detect the mode of the oscillator. Therefore, the command signal can simply be calculated as follows:

$$\begin{cases} \text{Trip} = 0 & if\ \{h_3(y) - h_4(y) < threshold\} \\ \text{Trip} = 1 & if\ \{h_3(y) - h_4(y) > threshold\}\ \&\{T > \text{Delay}\} \end{cases}.$$

The $h_n(y)$ shows the nth harmonic of the y signal, and the value of the *threshold* is considered to properly distinguish between normal and islanding conditions. In this paper, the best value for the *threshold* was found by trial and error as 0.13.

Another problem is that based on the aforementioned algorithm, the changing mode from chaotic motion to the great periodic motion even occurs during the grid-connected mode with

TABLE II
LOAD PARAMETERS FOR DIFFERENT Q_F

Q_f	R (Ω)	L (μH)	C (μF)	Resonant Frequency (Hz)	Quality of Detection
0.5	2.304	12200	575.4	60.0697	HD*
0.96	**2.304**	**6304.2**	**1115.9**	**60.0059**	**VHD****
1.57	**2.304**	**3875**	**1815.4**	**60.006**	**VHD**
2.12	2.304	2880	2439	60.0507	HD
3	2.304	2030	3452	60.1225	SD***
4.2	2.304	1450	4833.5	60.1181	SD

*HD = Hard to Detect; **VHD = Very Hard to Detect;
***SD = Simple to Detect.

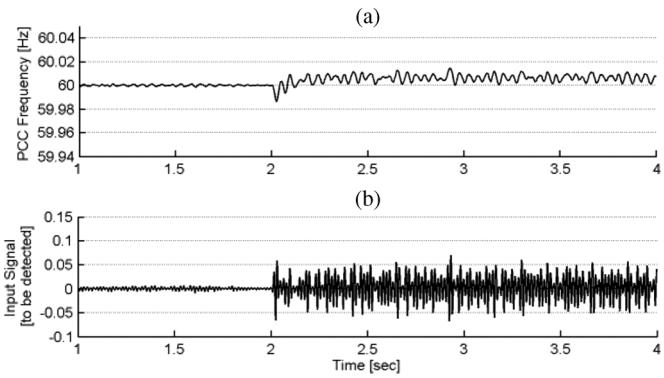

Fig. 5. Load quality factor test for $Q_f = 1.57$. (a) PCC frequency. (b) Duffing input signal.

load switching. But under such conditions, the state of the oscillator changes back to the chaotic motion in about 0.5 s. As a result of avoiding nuisance tripping, a delay time (*Delay*) was also considered in the algorithm. In Fig. 3, T is the instant time of the timer. By triggering the timer, T will count from zero to *Delay*. The size of this time delay was calculated based on load switching under the normal operation of the system. The Delay time was found by trial and error in all simulations (some presented in Section V) as 0.5 s.

V. PERFORMANCE EVALUATION

The system described in Section III and shown in Fig. 2 is modeled in the MATLAB/Simulink environment to evaluate the proposed method. The system and DG parameters are listed in the Appendix.

In all of the simulations, the parameter I_{qref} was set to 0 representing the unity power factor condition. In this section, the performance of the proposed islanding detection method should be evaluated for various loading conditions, load quality factors, load imbalance condition, and load switching.

A. Effect of Load Quality Factor

The UL 1741 test specifies that an islanding detection method must succeed in detecting the islanding phenomenon within 2 s for RLC loads with $Q_f \leq 1.8$ [2]. For the system shown in Fig. 2, the islanding condition was introduced at $t = 2$ s and the load quality factor was changed from 0.5 to 4.2 by adjusting the load inductance and capacitance according to Table II. The last column of this table, namely, "Quality of Detection" shows the impact of the frequency deviation of all loading conditions

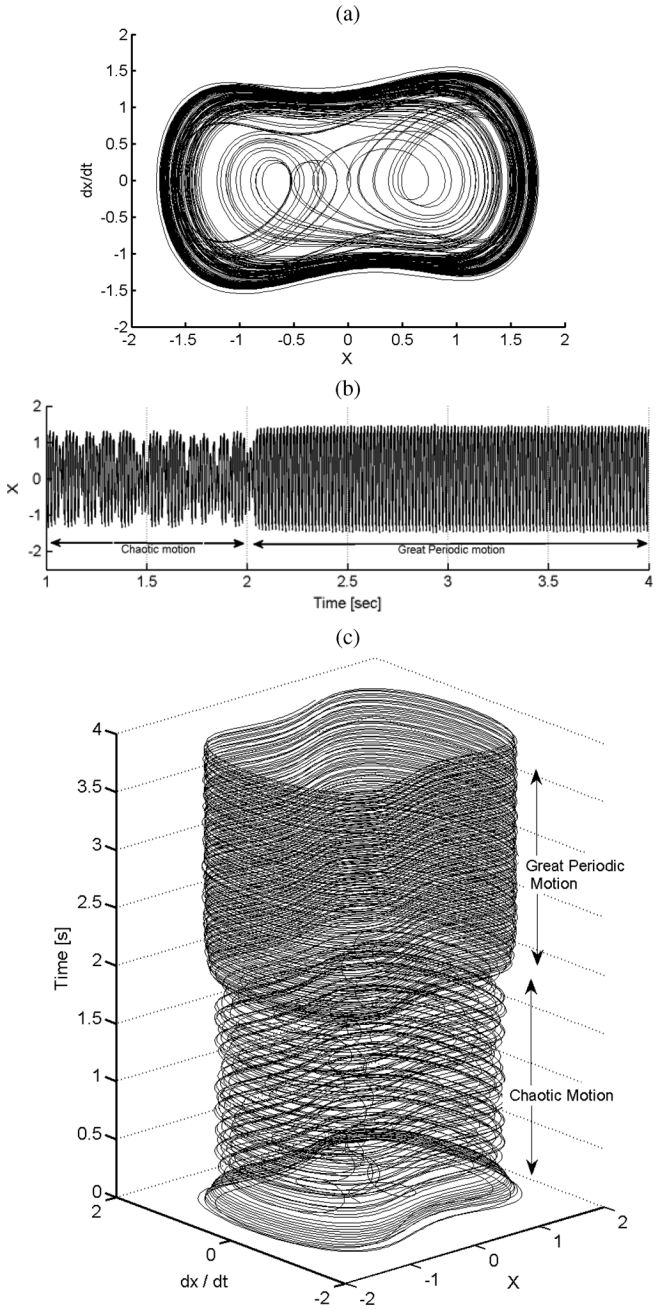

Fig. 6. Duffing oscillator outputs for $Q_f = 1.57$. (a) Phase plane diagram (top view). (b) $x - t$ diagram (side view). (c) 3-D view of the Duffing oscillator.

("Resonant Frequency" column) on the islanding detection process.

Fig. 5 shows the PCC frequency and input signal of the Duffing oscillator for $Q_f = 1.57$. This is one of the hardest loading conditions due to its nearby load resonance frequency and system frequency. Fig. 6 reveals the top view, $x - t$ diagram and the 3-D view of the proposed method for a better illustration of the Duffing oscillator mode changing process under the same loading conditions. Fig. 6(b) and (c) shows that for $t \leq 2$ s (grid-connected mode), the Duffing oscillator works normally in the chaotic motion, but after islanding ($t > 2$ s), due to the appearance of frequency deviation on PCC, the oscillator changes to the great periodic motion mode. Such a change results in a trip signal for disconnecting (using FFT

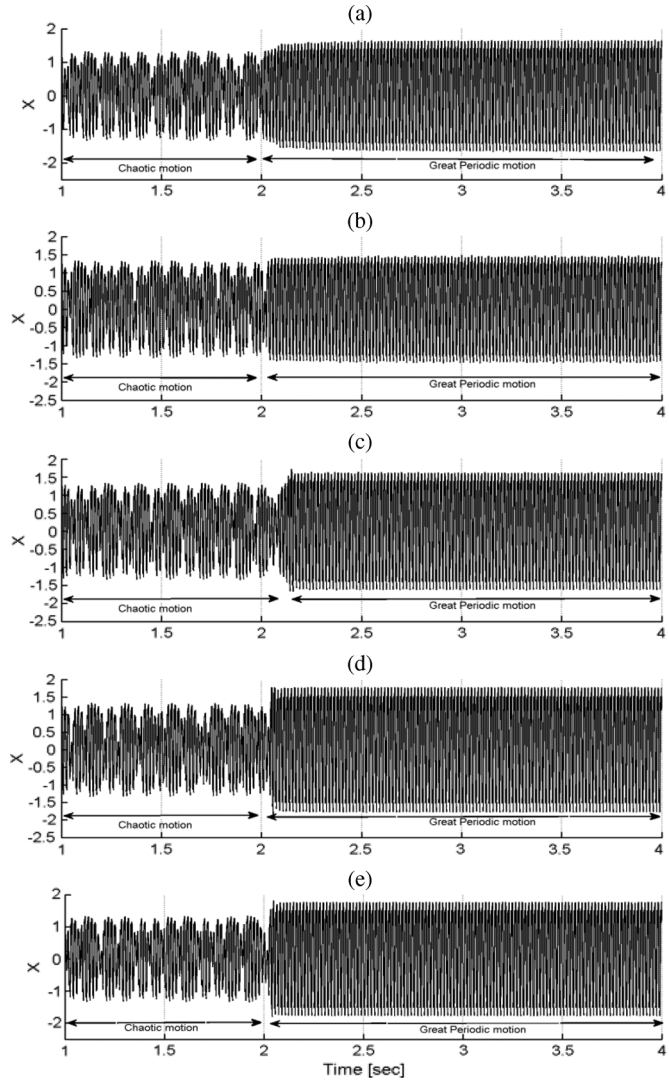

Fig. 7. Duffing oscillator $x - t$ diagram for different load quality factor tests. (a) $Q_f = 0.5$. (b) $Q_f = 0.96$. (c) $Q_f = 2.12$. (d) $Q_f = 3$. (e) $Q_f = 4.2$.

as discussed in the previous section) or adjusting the control strategy of the DG. The results for the remaining loading conditions, listed in Table II, are shown in Fig. 7. All of the test results revealed that the presented method is capable of detecting the islanded system in a fraction of a second (using normal PC and MATLAB software for the worse scenario, it takes about 0.1 s) to detect the change of the state of the Duffing oscillator. As a result, the total time (the detection time plus the deliberate Delay time) would be about 0.6 s, which is well below the standard, which is 2 s [2].

B. Effect of Load Switching

The proposed islanding detection method is tested for load switching in the grid-connected operation mode. In parallel with the load, shown in Fig. 2, a new load is switched at $t = 2$ s and disconnected at $t = 3$ s. In this regard, three cases have been simulated. In all cases, the load apparent power is equal to 100 kVA but the power factor is 0.8 lead, and 1.0 and 0.8 lag.

The PCC frequency, input signal of the Duffing oscillator, and Duffing oscillator output for the load with $Q_f = 1.57$, and

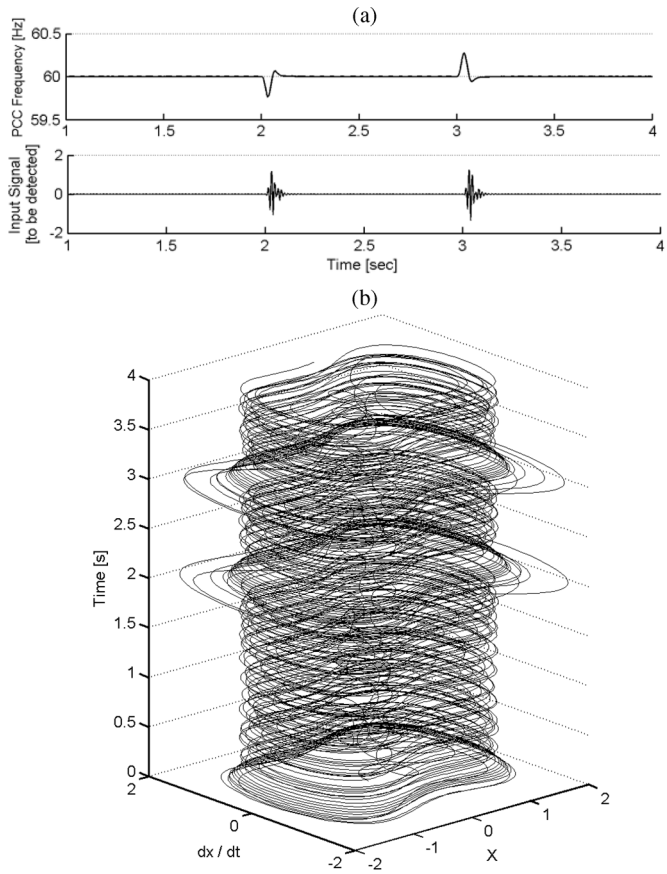

Fig. 8. Duffing oscillator outputs for load switching. (a) PCC frequency and input signal. (b) 3-D view of the Duffing oscillator.

switchable load (S = 100 [kVA]and 0.8 lead) are presented in Fig. 8. For the simulated cases, the voltage and frequency deviations are within the standard threshold values. It can be seen from Fig. 8(b) that when the system is in the grid-connected mode, the state of the Duffing oscillator is in the chaotic motion and when the second load is connected to the system (in the grid-connected mode), some frequency deviation appears in the PCC frequency due to the system equivalent impedance change. Therefore, the proposed method tries to change the state of the Duffing oscillator to the great periodic motion. Yet, the duration of transients is not enough to make a change in the state of the oscillator.

In this part of the paper, it is shown that the proposed method does not have a malfunction in the normal power system operation. Two other cases (not shown in this paper) had similar conclusions.

C. Effect of Load Imbalance

In this case study, all conditions comply with the UL 1741 test except that the load resistance is not balanced [26]. The procedure, presented in [8] and [26] for analyzing load unbalance, is applied. The tested load for this case has $Q_f = 1.57$. As listed in Table II, this case is very hard to detect. The unbalance in the load is created by varying the load-phase resistance. Two cases are considered: in case 1, only the resistance of the phase A is set to 90% of its rated value, and in case 2, the resistances of

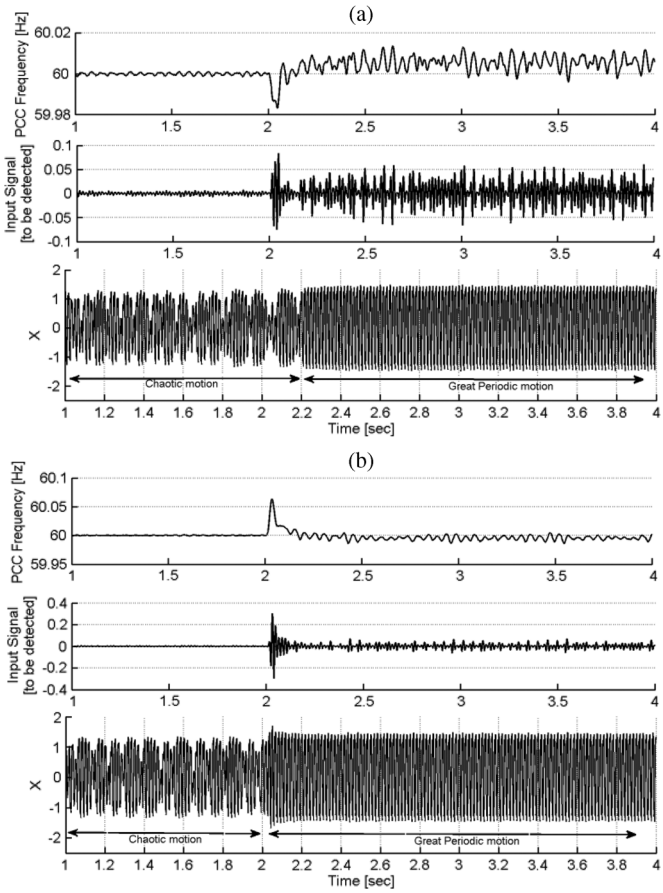

Fig. 9. System and Duffing oscillator outputs under the load imbalance condition. (a) Case 1. (b) Case 2.

phase A and C are set at 90% and 125% of the rated value, respectively. The islanding is modeled by disconnecting the grid at $t = 2$ s.

Fig. 9 presents the PCC frequency, the Duffing input signal, and the Duffing output signal for two cases. In Fig. 9(a), it can be seen that for the Duffing oscillator, it takes more time (about 0.2 s) to change from chaotic motion to great periodic motion due to less injection of the negative component in the system voltage (2%). For the second case in Fig. 9(b), it takes less time for the Duffing oscillator to change from chaotic motion to great periodic motion for 5% negative component in the system voltage. As a result, it can be concluded that the algorithm works better with the system containing higher values of load imbalance.

Based on the simulation results, the proposed islanding detection strategy functions correctly and will be capable of detecting islanding in less than a second for the presented loading cases.

D. Influence of Noise on the Duffing Input Signal

All simulations to this point were deduced based on the ideal measurement, and without any noise pollution. Fig. 10 shows the same signals of Fig. 6, while the measured signals are contaminated with a Gaussian white noise of $(\mathrm{SNR})_{\mathrm{i}} = 20\log(\mathrm{a}^2/4\sigma^2)$ [22].

Substituting $a = 0.0084$ and $\sigma = 0.0229$ in the $(\mathrm{SNR})_{\mathrm{i}}$, results in the maximum value of the signal-to-noise ratio (SNR) [i.e., -68 (dB)]. For the SNR above this value, the method

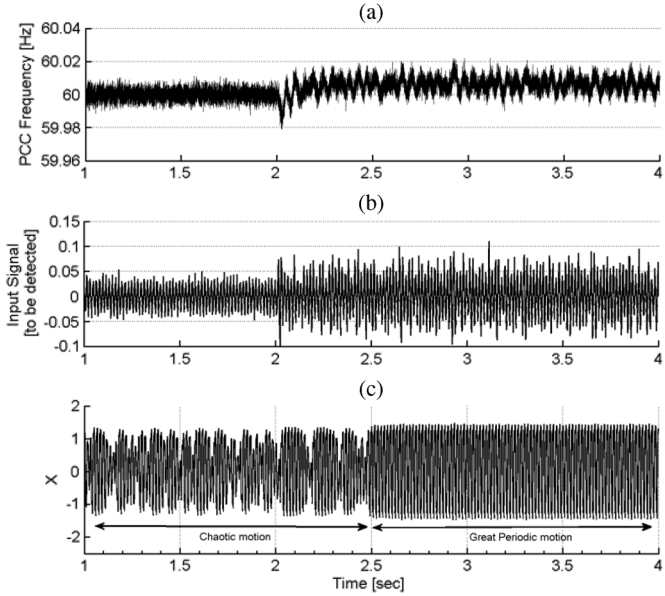

Fig. 10. Sensitivity-to-noise ratio test. (a) PCC frequency. (b) Duffing input signal. (c) $x - t$ diagram.

hardly or may not detect the islanding time. Also, Fig. 10 shows the effectiveness of the proposed method for one of the hardest loading conditions (listed in Table II) due to its nearby load resonance frequency to the system frequency. For the loading condition with greater frequency deviation, after islanding formation even with more SNR, the method could detect islanding timely. For the systems with high polluted measurement channels, the amount of k_f has to be tuned based on the magnitude of the measured noise.

E. NDZ of the Proposed Method

In most cases, there is always some active/reactive power mismatch between the DG output and the load. When the system is in the grid-connected mode, the power mismatch is provided by the grid. When the grid is disconnected, the voltage and frequency would be forced to new values due to the relation between active/reactive power and the system voltage and frequency.

The equations between the power mismatch (ΔP and ΔQ) and the PCC voltage and frequency can be found in [27] for the constant current-controlled DG

$$\Delta P = \pm 3\ \mathrm{V} \cdot \Delta V \cdot I \tag{24}$$

$$\Delta Q = \frac{3V^2}{\omega_n L}\left(1 - \frac{f_n^2}{(f_n \pm \Delta f)^2}\right). \tag{25}$$

These equations determine the zone, where the over/undervoltage protection and over/underfrequency protection would fail to detect islanding. For the voltage range of 88% to 110%, the amount of active power mismatch calculated by (24) is equal to 12.9 kW and 10.4 kW, respectively. The values of the reactive power mismatch for a frequency threshold in the range of 59.3 Hz to 60.5 Hz are 5.1 and 3.1 kVAR, respectively.

Now, for determining the NDZ of the proposed method, the frequency deviation (Δf) has to be calculated by (23), and the result should be substituted in (25) for determining the reactive

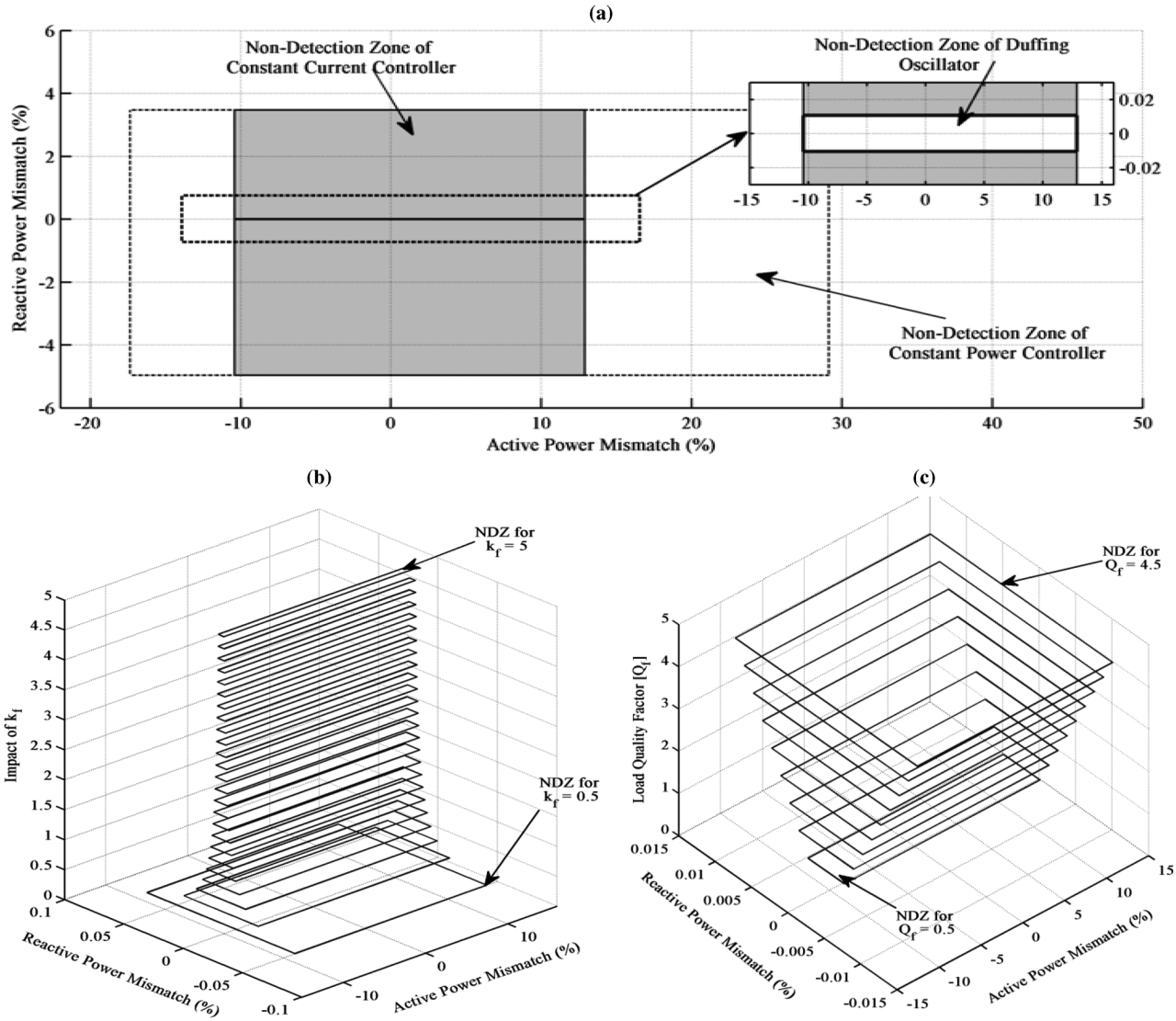

Fig. 11. NDZ evaluation of the proposed method. (a) NDZ of the OFP/UFP and OVP/UVP for two different types of inverter controllers in comparison with NDZ of the proposed method. (b) NDZ sensitivity analysis for $Q_f = 1$ and $k_f = [0.5 : 0.2 : 5]$. (c) NDZ sensitivity analysis for $Q_f = [0.5 : 0.5 : 5]$ and $k_f = 5$.

power mismatch. Since the method does not use the voltage in the detection process, the active power mismatch is the same as the OVP/UVP thresholds. The reactive power mismatch is calculated, as follows:

$$\Delta Q = \frac{3V^2}{\omega_n L}\left(1 - \frac{f_n^2}{\left(f_n \pm \left(\frac{\gamma - \gamma_c - \Delta f_0}{k_f}\right)\right)^2}\right) \tag{26}$$

where γ_c and Δf_0 are listed in Table I. Also, γ must be equal to γ_{th} for evaluating the threshold for each k_f. Fig. 11(a) shows the NDZ of the proposed method compared to the OVP/UVP and OFP/UFP for constant current and constant power controllers. In this figure, the active/reactive power mismatch is plotted based on the percentage of the system active power (100 kW in this paper). In Fig. 11(a), the simulation parameters are $k_f = 5$ and the load quality factor is equal to 1. The NDZ of the proposed method has been shown to be very tiny and could be neglected, differentiating the OVP/UVP and OFP/UFP zone for constant current and constant power controllers.

Moreover, Fig. 11(b) and (c) shows the NDZ sensitivity analysis for Q_f and k_f. In Fig. 11(b), Q_f is equal to 1 and k_f changes from 0.5 to 5 with a step change of 0.2. Fig. 11(c) is also formed by keeping k_f equal to 5 and changing Q_f from 0.5 to 4.5 with a step change of 0.5. Considering Fig. 11(b) and (c), it can be concluded that the NDZ of the proposed method is subject to the frequency deviation rather than the load quality factor.

VI. Conclusion

This paper proposes a new passive islanding detection method of inverter-based DG units, which can detect the weak signal by using the Duffing oscillator. The Duffing equation has been applied because it is one of the classic nonlinear systems that has been extensively studied. The basic idea is that a small periodic signal in noise can be detected by the Duffing oscillator via a transition from the chaotic motion to great periodic motion and vice versa. The proposed islanding detection method has also been studied under different load quality factors; imbalance loading conditions and load switching. The

influence of the noise on the quality of the detection has also been tested. The mathematical formulation and numerical simulations confirmed that the NDZ of the proposed method is very tiny and could be neglected. The simulation results show that applying the proposed method to the inverter-based DG, results in a simple, accurate and non-malfunction detection of islanding.

APPENDIX

Grid and Inverter Parameters	
DG rated output	120 kVA;
DG output power	100 kW;
Switching frequency	8 kHz;
Input dc voltage	900 V;
Voltage (line to line)	480 V;
System frequency (f)	60 Hz;
Grid resistance (R_s)	0.012 Ω;
Grid inductance (L_s)	0.3056 mH;
Filter inductance (L_f)	800 μH;
Filter resistance (R_{Lf})	0.004 Ω;
Filter capacitance (C_f)	30 μF;
Filter resistance (R_{cf})	1 Ω;
DG constant current controller parameters	
I_d control	$K_p = 0.2$, $K_i = 100$;
I_q Control	$K_p = 0.2$, $K_i = 100$.

REFERENCES

[1] *IEEE Standard for Interconnecting Distributed Resources With Electric Power Systems*, IEEE Standard 1547-2003, Jul. 2003.

[2] Underwriters Laboratories, Inc., "Static inverter and charge controllers for use in photovoltaic systems" Northbrook, IL, 2001, Standard UL.

[3] R. H. Lasseter and P. Paigi, "Microgrid: A conceptual solution," in *Proc.IEEE 35th Power Electron. Specialists Conf.*, Jun. 2004, vol. 6, pp. 4285–4290.

[4] J. Liang, T. C. Green, G. Weiss, and Q. Zhong, "Hybrid control of multiple inverters in an island-mode distribution system," in *Proc. IEEE 34th Annu. Power Electron. Specialist Conf.*, Jun. 2003, vol. 1, pp. 61–66.

[5] F. Katiraei and M. R. Iravani, "Power management strategies for a microgrid with multiple distributed generation units," *IEEE Trans. Power Syst.*, vol. 21, no. 4, pp. 1821–1831, Nov. 2008.

[6] S. Barsali, M. Ceraolo, P. Pelacchi, and D. Poli, "Control techniques of dispersed generators to improve the continuity of electricity supply," *Proc. IEEE Power Eng. Soc. Winter Meeting*, vol. 2, pp. 789–794, 2002.

[7] M. Ropp and W. Bower, "Evaluation of islanding detection methods for photovoltaic utility interactive power systems," Int. Energy Agency Implementing Agreement Photovoltaic Power Syst., Tech. Rep. IEA PVPS T5-09, Mar. 2002.

[8] H. H. Zeineldin, "A $Q - f$ droop curve for facilitating islanding detection of inverter-based distributed generation," *IEEE Trans. Power Electron.*, vol. 24, no. 3, pp. 665–673, Mar. 2009.

[9] H. H. Zeineldin and J. L. Kirtley, "A simple technique for islanding detection with negligible nondetection zone," *IEEE Trans. Power Del.*, vol. 24, no. 2, pp. 779–786, Apr. 2009.

[10] F. De Mango, M. Liserre, and A. D. Aquila, "Overview of anti islanding algorithms for PV systems. Part II: Active methods," in *Proc. IEEE Power Electron. Motion Control Conf.*, Jan. 2007, pp. 1884–1889.

[11] M. A. Redfern, O. Usta, and G. Fielding, "Protection against loss of utility grid supply for a dispersed storage and generation unit," *IEEE Trans. Power Del.*, vol. 8, no. 3, pp. 948–954, Jul. 1993.

[12] W. Freitas, W. Xu, C. M. Affonso, and Z. Huang, "Comparative analysis between ROCOF and vector surge relays for distributed generation applications," *IEEE Trans. Power Del.*, vol. 20, no. 2, pt. 2, pp. 1315–1324, Apr. 2005.

[13] J. C. M. Vieira, W. Freitas, W. Xu, and A. Morelato, "Efficient coordination of ROCOF and frequency relays for distributed generation protection by using the application region," *IEEE Trans. Power Del.*, vol. 21, no. 4, pp. 1878–1884, Oct. 2006.

[14] H. Shyh-Jier and P. Fu-Sheng, "A new approach to islanding detection of dispersed generators with self-commutated static power converters," *IEEE Trans. Power Del.*, vol. 15, no. 2, pp. 500–507, Apr. 2000.

[15] S. K. Salman, D. J. King, and G. Weller, "New loss of mains detection algorithm for embedded generation using rate of change of voltage and changes in power factors," in *Proc. Inst. Elect. Eng. Develop. Power Syst. Protect. Conf.*, 2001, pp. 82–85.

[16] B. Singam and Y. Huil, "Assessing SMS and PJD schemes of anti-islanding with varying quality factor," in *Proc. IEEE Power Energy Conf.*, Nov. 2006, pp. 196–201.

[17] S. Jang and K. Kim, "An islanding detection method for distributed generations using voltage unbalance and total harmonic distortion in current," *IEEE Trans. Power Del.*, vol. 19, no. 2, pp. 745–752, Apr. 2004.

[18] B.-G. Yu, M. Matsui, and G.-J. Yu, "A correlation-based islanding-detection method using current-magnitude disturbance for PV system," *IEEE Trans. Ind. Electron.*, vol. 58, no. 7, pp. 2935–2943, Jul. 2011.

[19] F. Liu, Y. Kang, S. Duan, and X. Lin, "Improved SMS islanding detection method for grid-connected converters," *Inst. Eng. Technol. Renew. Power Gen.*, vol. 4, no. 1, p. 36042, 2010.

[20] L. A. C. Lopes and H. Sun, "Performance assessment of active frequency drifting islanding detection methods," *IEEE Trans. Energy Convers.*, vol. 21, no. 1, pp. 171–180, Mar. 2006.

[21] M. E. Ropp, M. Begovic, A. Rohatgi, G. A. Kern, R. H. Bonn, and S. Gonzalez, "Determining the relative effectiveness of islanding detection methods using phase criteria and nondetection zones," *IEEE Trans. Energy Convers.*, vol. 15, no. 3, pp. 290–296, Sep. 2000.

[22] G. Wang, D. Chen, J. Lin, and X. Chen, "The application of chaotic oscillator to weak signal detection," *IEEE Trans. Ind. Electron.*, vol. 46, no. 2, pp. 440–444, Apr. 1999.

[23] G. Wang and S. He, "A quantitative study on detection and estimation of weak signals by using chaotic duffing oscillators," *IEEE Trans. Circuits Syst. I, Fundam. Theory Appl.*, vol. 50, no. 7, pp. 945–953, Jul. 2003.

[24] N. Q. Hu and X. S. Wen, "The application of duffing oscillator in characteristic signal detection of early fault," *J. Sound Vibr.*, vol. 268, no. 5, pp. 917–931, Dec. 2003.

[25] H. Vahedi, R. Noroozian, A. Jalilvand, and G. B. Gharehpetian, "A new method for islanding detection of inverter-based distributed generation using DC-link voltage control," *IEEE Trans. Power Del.*, vol. 26, no. 2, pp. 1176–1186, Apr. 2011.

[26] H. Karimi, A. Yazdani, and R. Iravani, "Negative-sequence current injection for fast islanding detection of a distributed resource unit," *IEEE Trans. Power Electron.*, vol. 23, no. 1, pp. 298–307, Jan. 2008.

[27] H. H. Zeineldin, E. F. El-Saadany, and M. M. A. Salama, "Impact of DG interface control on islanding detection and nondetection zones," *IEEE Trans. Power Del.*, vol. 21, no. 3, pp. 1515–1523, Jul. 2006.

Hesan Vahedi (S'12) received the M.S. (Hons.) degrees in electrical engineering from Zanjan University (ZNU), Zanjan, Iran, in 2010 and is currently pursuing the Ph.D. degree in electrical engineering from Amirkabir University of Technology (AUT), Tehran, Iran.

His main research interests include control systems, applications of power electronics in power systems, distributed generation, and artificial intelligence.

G. B. Gharehpetian (SM'08) received the Ph.D. degree (Hons.) in electrical engineering from the University of Tehran, Tehran, Iran, in 1996.

He was Assistant Professor at Amirkabir University of Technology, Tehran, from 1997 to 2003, and Associate Professor from 2004 to 2007. He has been a Professor since 2007. He is the author of more than 450 journal and conference papers. His teaching and research interests include power system and transformers transients and power-electronics applications in power systems.

Prof. Gharehpetian is a senior and distinguished member of the Iranian Association of Electrical and Electronics Engineers (IAEEE), respectively, and a member of the central board of IAEEE. He was selected by the Ministry of Higher Education as the Distinguished Professor of Iran and by the IAEEE as the Distinguished Researcher of Iran and was awarded the National Prize in 2008 and 2010, respectively.

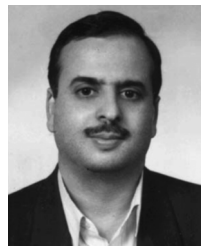

Mehdi Karrari received the Ph.D. degree in control engineering from Sheffield University, Sheffield, U.K., in 1991.

Since 1991, he has been with the Amirkabir University of Technology, Tehran, Iran. He is the author or coauthor of more than 100 technical papers and one book: *Power System Dynamics and Control* (2004), in Persian. His main research interests are power system modeling, modeling and identification of dynamic systems, and large-scale and distributed systems.